



# Back stress and strength contributions evolution of a heterogeneous austenitic stainless steel obtained after one pass by equal channel angular sheet extrusion (ECASE)

Jairo Alberto Muñoz<sup>1,2</sup> · Alexander Komissarov<sup>2</sup>

Received: 24 April 2020 / Accepted: 8 June 2020 / Published online: 17 June 2020  
© Springer-Verlag London Ltd., part of Springer Nature 2020

## Abstract

This research work studies the different strength contributions of a sheet-shaped heterogeneous austenitic stainless steel, after having been processed at room temperature by one ECASE pass. A significant hardness increase was found throughout its thickness, showing higher values near the edges while the middle area presents the smallest gains. The material heterogeneity gives rise to a plastic gradient deformation between the soft and hard areas of the microstructure. As a consequence, a more significant amount of geometrically necessary dislocations concentrates on the interfaces of these areas, which helps the material to maintain a reliable strength-ductility ratio. After the dislocations contribution to the material strength, the second contribution comes from the back stress mechanism, followed by grain size contributions. All types of contributions were higher in the edge neighborhoods than in the middle zone. Unlike the contributions from dislocations and grain size that decrease as they approach the interfaces between the hard and soft areas, the back stress contribution does the opposite, showing high increments in these zones.

**Keywords** Phase transformation · Dislocations · Grain size · Hardness · Strength · Back stress

## 1 Introduction

The constant worldwide demand for materials with better mechanical characteristics that allow building parts and structural elements more efficiently and with a favorable cost-benefit ratio has led the scientific community to seek and develop new materials and processes. Within the new type of materials, materials with heterogeneous structures have begun to attract attention during the last 5 years [1, 2]. This type of materials has demonstrated an acceptable mixture of strength and ductility by combining different microstructural

characteristics such as abnormal grain size distributions, varied densities of dislocations, and different proportions of phases on the geometry of the piece among other features [3–6].

The excellent combination of strength and ductility presented by the heterogeneous materials can be explained by a process in which the deformation follows a complex behavior, especially at the interfaces between soft and hard areas, where geometrically necessary dislocations (GNDs) play an essential role by stacking and accumulating themselves around the interfaces creating a plastic deformation gradient [7, 8]. This behavior results in additional material hardening due to the deformation partition. Thus, first generated dislocations from the soft areas can stack in the interfaces of the hard zones. Because the soft areas deform plastically while the hard ones still do so elastically, avoiding the free sliding of dislocations. According to Li et al. [9], this mechanism known as back stress can even reach 600 MPa in some heterogeneous lamella-like structures.

Several authors have shown how heterogeneous structures are obtained through severe plastic deformation techniques such as equal channel angular pressing (ECAP) [10] and

✉ Jairo Alberto Muñoz  
munoz@ifir-conicet.gov.ar

Alexander Komissarov  
komissarov@mis.ru

<sup>1</sup> Instituto de Física Rosario, Consejo Nacional de Investigaciones Científicas y Técnicas-CONICET, Universidad Nacional de Rosario, Ocampo y Esmeralda, 2000 Rosario, Argentina

<sup>2</sup> National University of Science and Technology “MISIS”, Moscow 119049, Russia

high-pressure torsion (HPT) [11]. Although, perhaps the most widely used techniques for obtaining heterogeneous structures have been those that only affect the material's surface [12–16]. Techniques such as shoot penning [13–15] and severe impact [17] have shown to be useful in modifying mainly the material surface, trying to preserve its core without deformation, thus having a sandwich structure with a soft core surrounded by two hard layers.

Similarly, severe plastic deformation techniques such as ECAP can be adapted to produce heterogeneous structures like the sandwich type. To achieve this goal is necessary to control the deformation of the process between each ECAP pass by equivalent deformations of lower intensity (i.e., higher internal ECAP die angles) and thus be able to make evident the localized shearing effect that mainly affects the sheet metal edges as previous studies demonstrate it [18]. So far, there have been very few studies of the ECASE feasibility in the processing of metallic materials with a flat geometry, because most of them focus on obtaining ultra-fine grain structures. For that reason, their final goal is just introducing large deformations [19–21].

Austenitic stainless steels (ASSs) present attractive characteristics due to their deformation mechanisms depending on their stacking fault energy (SFE). These materials are well known for their excellent mechanical properties as well as corrosion resistance, among other properties [22, 23]. In this way, one of the most important characteristics that allow showing the material heterogeneity induced through the ECASE process is the phase change induced by deformation, when changing from metastable austenite fcc to martensite bcc. This mechanism is favored when the material has a low SFE and is deformed at room temperature or lower temperatures because the metastability of these steels increases as their SFE decreases. Mainly, austenitic stainless steels of the 304L series are one of the most sensitive materials to this phase change [24].

There are also other types of mechanisms that contribute to the metallic materials hardening and that influence the mechanical properties of the steel considered in this study; such contributions come from the solid solution, grain size, dislocations, and as a new mechanism the back stress. The first three have been extensively studied while the last one is still under study. Hence, to better understand the mechanical behavior of heterogeneous materials, it is necessary to understand the evolution of each of the hardening mechanisms within the heterogeneous structure. However, although several studies have been carried out lately regarding the strength evolution of heterogeneous structure materials [9, 11, 25, 26], few studies show the evolution of each of these mechanisms on the interfaces that make up this type of structures.

Therefore, the main objective of this study is to quantify each of the strength contributions for a heterogeneous austenitic stainless steel processed at room temperature by ECASE.

For which, the microstructural evolution and mechanical properties across the sheet thickness will be studied by electron back scattering diffraction (EBSD), hardness, and uniaxial tensile tests. In this way, changes in grain size, percentage of phases, and dislocation densities will be obtained as a function of sheet thickness, allowing to know each of the hardening components at each point of the sheet thickness and for each phase.

## 2 Experimental procedure

The steel received in the form of sheet 20 mm wide, 5 mm thick, and 120 mm long was water quenched after being maintained for 2 h at a temperature of 850 °C. The steel composition in weight percentage was 0.03C, 17.5Cr, 2Mn, 8Ni, 0.045P, 1Si, 0.03S, and Fe as balance. According to this composition and the equation proposed by Schramm et al. [27], the SFE would be  $\sim 15.25 \text{ mJ/m}^2$ , which is considered a low SFE where martensitic transformation is the preferred deformation mechanism [28, 29]. Subsequently, the material was deformed by ECASE using a die with an internal angle of 150° (see Fig. 1), which confers the material a real strain of 0.31 according to the equation of Iwahashi et al. [30].

Digital image correlation (DIC) was employed to obtain deformation map measurements on tensile specimens. With this technique, a speckle pattern is painted on the gauge length of the samples to be tested and then the deformation is determined through the relative change in the shape and position of the different random spot patterns.

Mechanical characterization was carried out by tensile tests and hardness measurements. A load of 0.98 N with a dwell period of 15 s was used for the Vickers hardness. Bone-shaped tensile samples (gauge dimension of 12 mm × 3.9 mm × 4.4 mm and 12 mm × 3.9 mm × 1 mm for samples around the edge and middle zones) were cut through the sheet thickness and tested at a constant strain rate of  $1.1 \times 10^{-3} \text{ s}^{-1}$ .

A scanning electron microscope (SEM) coupled with an electron backscatter diffraction (EBSD) detector operating at

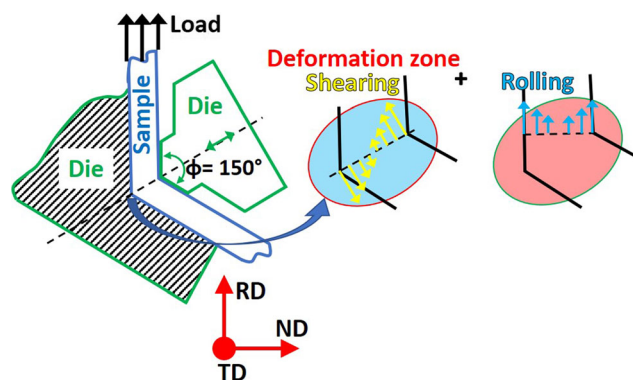


Fig. 1 ECASE process sketch

21 kV was used to characterize the microstructure. Microstructure heterogeneity displayed through 3 scans (1  $\mu\text{m}$  and 0.05  $\mu\text{m}$  step sizes) across the sheet thickness (4400  $\mu\text{m}$  after 1 ECASE pass), two near the edges (0–600  $\mu\text{m}$  and 3800–4400  $\mu\text{m}$  for the left and right edges zones, respectively), and one in the sheet core (1900–2500  $\mu\text{m}$ ) on the transversal direction (TD) plane. Grain mean orientations set as reference orientations and a half quadratic minimization filter with a threshold of  $1.5^\circ$  were used to denoise the data.

### 3 Results and discussion

#### 3.1 Microstructure evolution

In order to show the generation of a heterogeneous structure employing the ECASE process, it can be initially observed in Fig. 2 the microstructural evolution for the deformed material (Fig. 2a) and in its original state (Fig. 2b). Figure 2a shows how the deformed material presents an evident microstructural

change in the edge vicinities through a higher formation of martensite induced by deformation than in the sheet core. Additionally, Fig. 2c indicates the percentage of phase variation on the sheet thickness, showing a more significant fraction of the bcc phase at the edges of the sheet than the center zone. Meanwhile, the initial material (Fig. 2b) keeps the percentage of phases constant throughout the thickness.

Other microstructural characteristics such as grain size and the misorientation evolution also manifest a heterogeneous behavior. Figure 3 a and b highlight a bimodal behavior for the grain size where the areas near the edges register two characteristic peaks revealing zones with smaller grain sizes around the edges ( $< 20 \mu\text{m}$ ) and zones with sizes larger than  $40 \mu\text{m}$  located at 300- $\mu\text{m}$  distance from the edges.

Therefore, kernel average misorientation (KAM) measurements reveal a misorientation gradient over the piece thickness. Figure 3 c and d represent KAM maps as well as their variation on the thickness of the piece, respectively. Figure 3 d demonstrates that the highest KAM values extend to a length of  $\sim 600 \mu\text{m}$  on each side of the sheet. This behavior

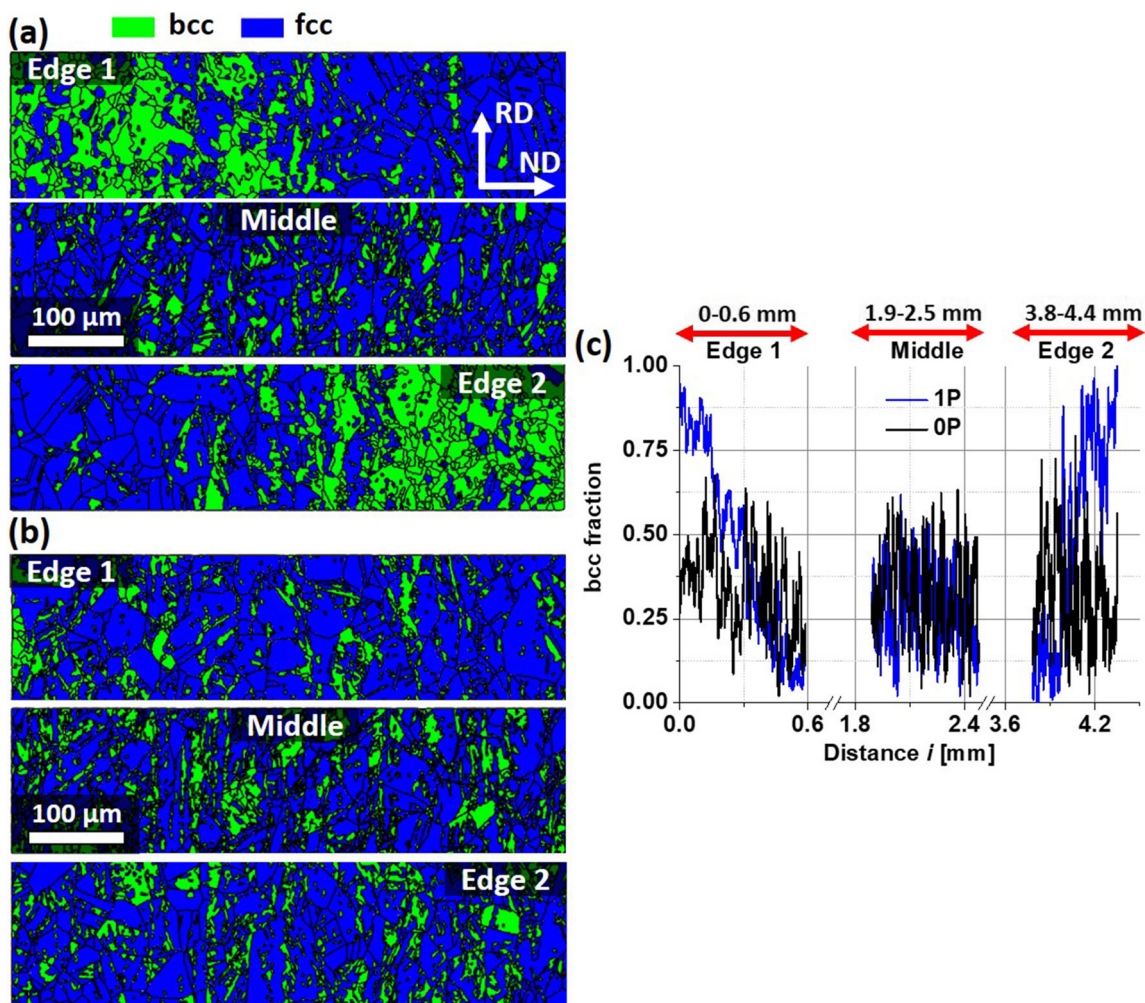


**Fig. 2** Microstructure characterization. EBSD phase maps (a) after 1 ECASE pass, (b) initial material, and (c) bcc phase variation along the sheet thickness

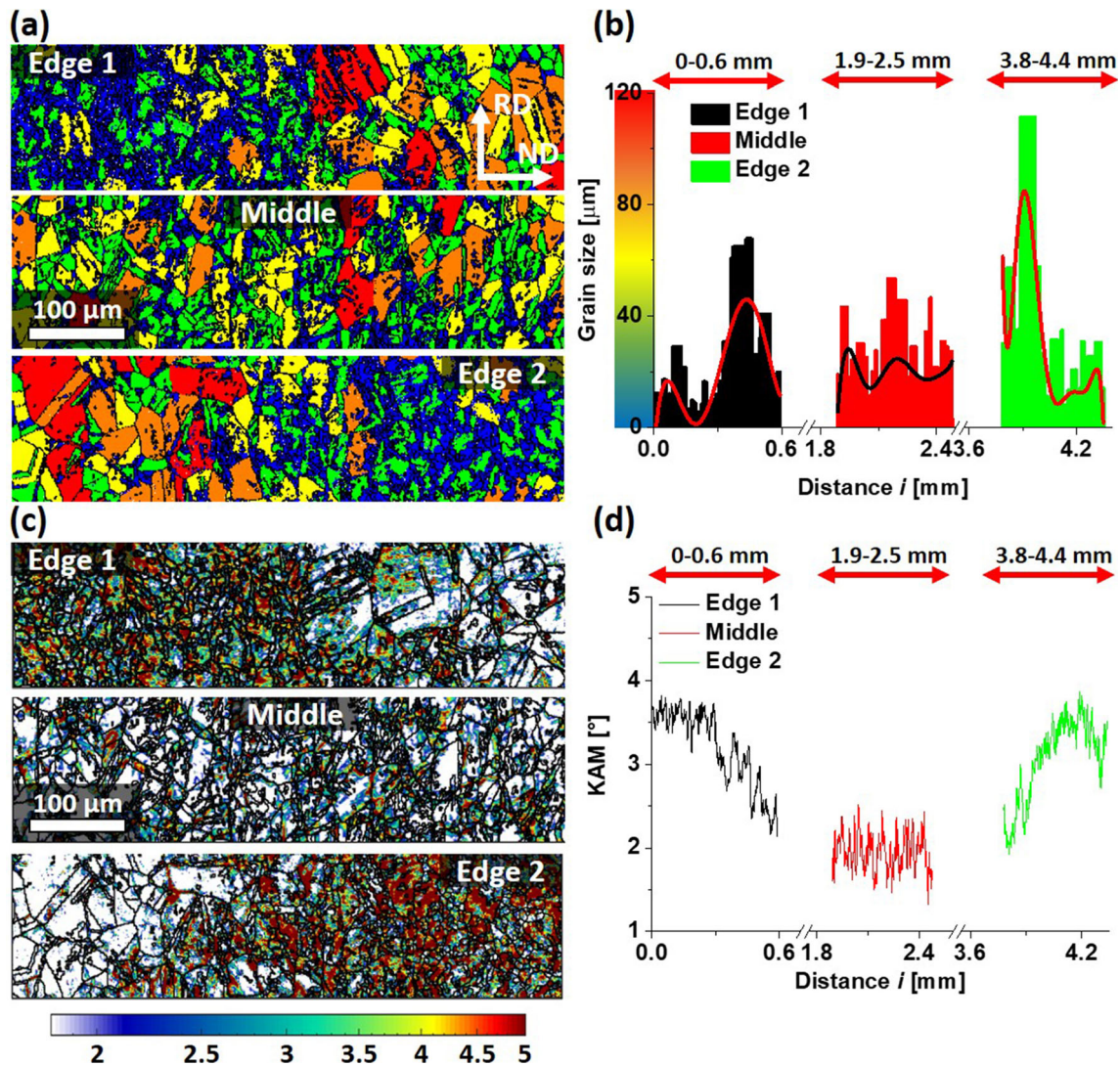


**Fig. 3** EBSD calculations for the heterogeneous material. (a) Grain size maps, (b) average grain size along the sheet thickness, (c) KAM maps, and (d) KAM values along the sheet thickness

demonstrates that the ECASE process generates a microstructural gradient starting with the region dominated by the phase transformation from austenite to martensite with a smaller grain size and high misorientations followed by a less deformed region between 300 and 600 μm where misorientations are still high, and ends with a region where the initial phases remain unchanged as Fig. 4 describes it. These observations confirm the formation of a structure formed by a soft region which is surrounded by two hard regions.

### 3.2 Mechanical properties

Figure 5 represents the hardness evolution, as well as the tensile behavior of the heterogeneous material. Figure 5 a indicates that the hardness over the sheet thickness for the initial material remains relatively

constant. In contrast, after one ECASE pass, the material shows a U-shaped hardness evolution with the highest values around the edge neighborhoods—allowing to appreciate that the most significant variations locate around 1 mm on each side of the sheet.

Figure 5 b shows the tensile curves for the heterogeneous material in different areas of the sheet. This figure shows how the curve corresponding to the area near the edge (1P Edge) possesses high strength and low ductility while the curve corresponding to the middle zone (1P Middle) presents not only the highest ductility but also the lowest strength, confirming the existence of a plastic gradient.

It is worth mentioning that the final strength-deformation combination (i.e., 650 MPa yield stress and 31% uniform deformation) stands out to those of

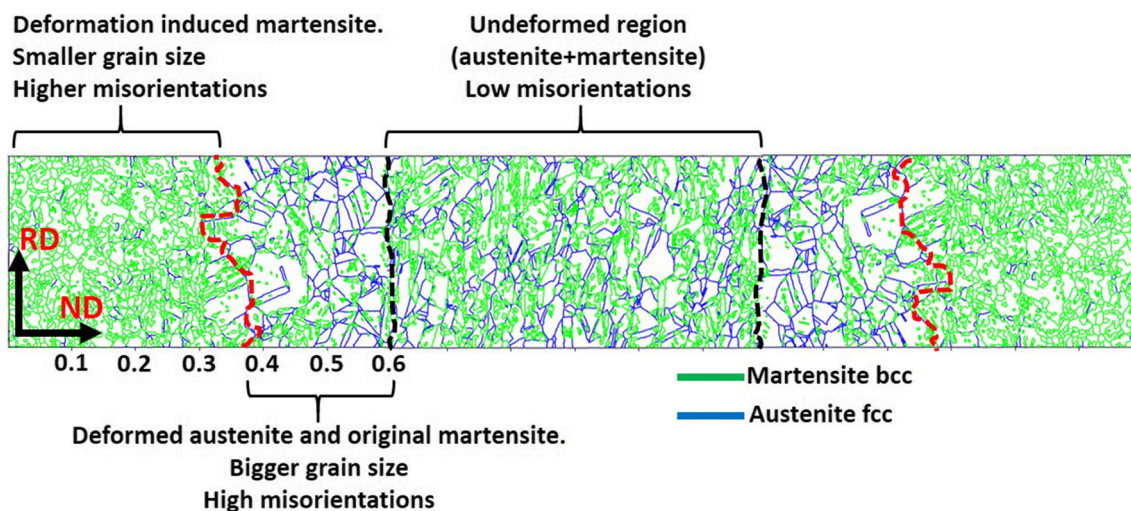


Fig. 4 Microstructure zones along the sheet thickness

other heterogeneous ASSs obtained by various and more exhaustive processing methods. E.g., Zheng et al. [31] reported 725 MPa and 35% uniform deformation after combining ECAP + annealing, while Park et al. [32] found 450 MPa and 38% uniform deformation in a harmonic structure.

### 3.3 Strengthening mechanisms of the heterogeneous material

To study the mechanical response of the heterogeneous material, the different zones that make up the material are analyzed using a Hall-Petch type equation, as shown below:

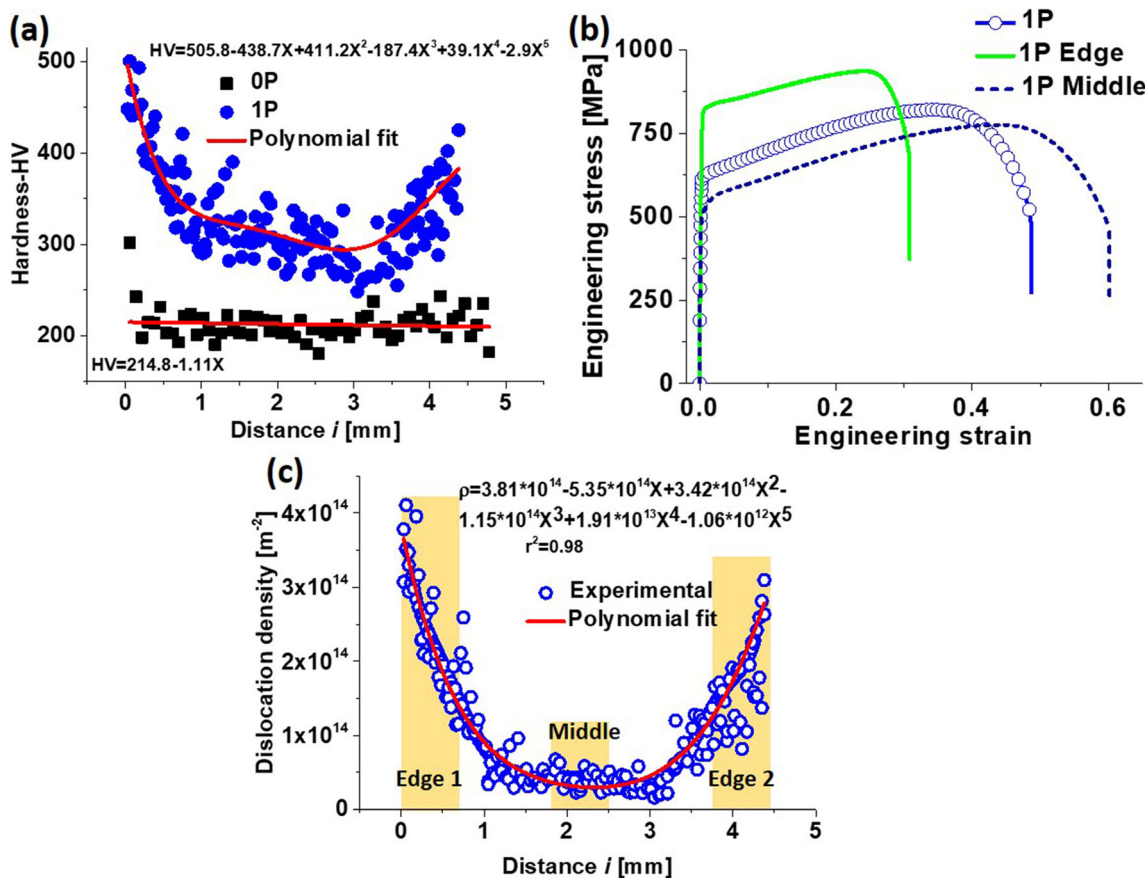
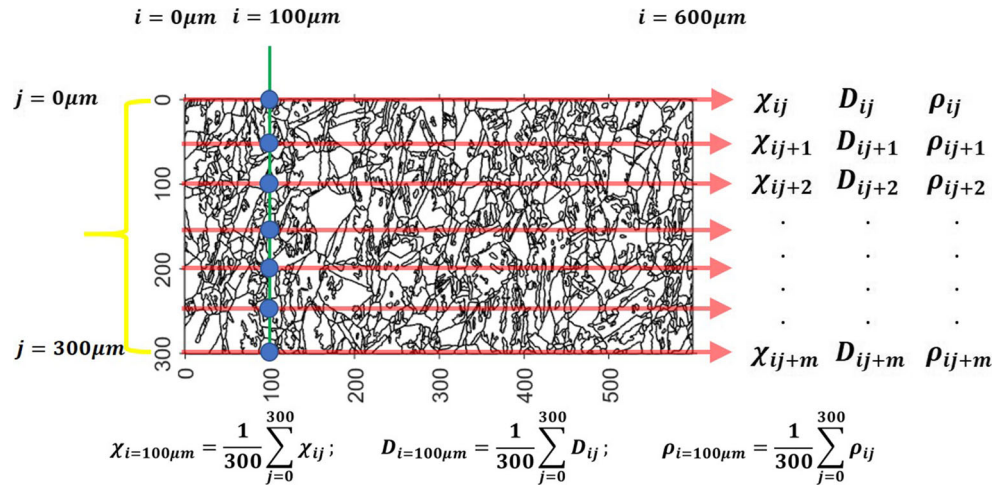


Fig. 5 Mechanical properties. (a) Hardness values on the TD plane, (b) stress-strain curves for the heterogeneous material, and (c) dislocation density evolution

**Fig. 6** Microstructure measurements (phase percentages— $\chi$ , grain size— $D$ , and dislocation densities— $\rho$ ) sketch



$$\sigma_y = \sigma_0 + K.D^{-1/2} + \alpha G M b \rho^{1/2} \tag{1}$$

where the first term takes into account Peierls’s stress and the solid solution hardening, the second term refers to the grain size contribution, and the third considers the dislocations contribution. For metallic materials like steels, Eq. (1) can also be expressed in terms of hardness, as indicated in Eq. (2):

$$H_y = H_0 + H_D + H_\rho \tag{2}$$

where  $H_y = \sigma_y/C$ ,  $H_0 = \sigma_0/C$ ,  $H_\rho = \sigma_\rho/C$ , with  $C$  as a constant. Therefore, considering the phase percentages variations, and the grain size evolution across the sheet thickness, strength contributions of each phase and zone can be estimated as an average of the sum over the material thickness. Consequently, the strength equations for Peierls and grain size are as follows:

$$\sigma_0 = \frac{1}{n} \cdot \sum_{i=0}^{600} [\chi_i \cdot \sigma_{0-bcc} + (1-\chi_i) \cdot \sigma_{0-fcc}] \tag{3}$$

$$\sigma_D = \frac{1}{n} \cdot \sum_{i=0}^{600} [\chi_i \cdot K_{bcc} \cdot D_i^{-1/2} + (1-\chi_i) \cdot K_{fcc} \cdot D_i^{-1/2}] \tag{4}$$

with  $\chi_i$  is the martensite fraction at a distance  $i$  measured from the sheet edge in the EBSD map and  $n$  represents the number

of measurements made on the length of each area, in this case, 600 measurements (each of them averaged over the scan width) over a 600- $\mu\text{m}$  length of each EBSD scan (see Fig. 6). On the other hand, the constant  $C$  values are obtained through the strength-hardness ratio for each zone according to the yield stresses and the corresponding hardness values of Fig. 5a. E.g., for the edge zone (from 0 to 600  $\mu\text{m}$ ), we consider the yield stress (1P edge from Fig 5b) and the hardness values around the edge. The same applies to the middle zone but considering the correct yield stress (1P middle from Fig. 5b) and the properly distance values (1890–2500  $\mu\text{m}$ ). In this way, by converting the hardness values in terms of stress, the dislocation density evolution can be obtained using the equation proposed by Taylor [33]:

$$\rho_i = \frac{1}{13.5} \left( \frac{H_{Vi} - H_{V0i}}{\alpha G M b} \right)^2 \tag{5}$$

where  $H_{Vi}$  and  $H_{V0i}$  represent the hardness values at different distances ( $i$ ) of the sheet thickness for both the deformed and the initial state material, respectively. Then, using the hardness evolutions presented in Fig. 5a together with their respective fitting curves, the parameters of Table 1 and Eq. (5), the dislocation density evolution curve can be visualized as a function of the sheet thickness, as Fig. 5c indicates.

Figure 7 a represents the evolution of the geometrically necessary dislocation through the EBSD measurements [38], taking into account the two phases. Figure 7 a also highlights the no-homogeneous behavior of both GNDs and statistical dislocations with high scattering over the plate thickness. At first glance, Fig. 7 a indicates that the dislocation densities are much higher in the edge neighborhoods than any other region with values decreasing from  $8 \times 10^{14} \text{ m}^{-2}$  to  $3 \times 10^{14} \text{ m}^{-2}$  as it moves away from these areas. Beyond 600  $\mu\text{m}$ , it reaches a stable behavior in the middle area with densities between  $1 \times 10^{14}$  and  $3 \times 10^{14} \text{ m}^{-2}$ . Concerning the GNDs, it can be distinguished that in the areas near the edge, the highest densities

**Table 1** Material constant values used to calculate the strength contributions

Parameter	bcc	fcc	Reference
$\sigma_0$ (MPa)	122.2	180	[34, 35]
$K$ (Mpa·m <sup>1/2</sup> )	0.36	0.24	[34, 36]
$\alpha$	0.3		[36]
$M$	3.05		[37]
$b$ (m)	$\sqrt{3}a/2$	$\sqrt{2}a/2$	
	with $a$ as the lattice parameter		
$G$ (GPa)	77		

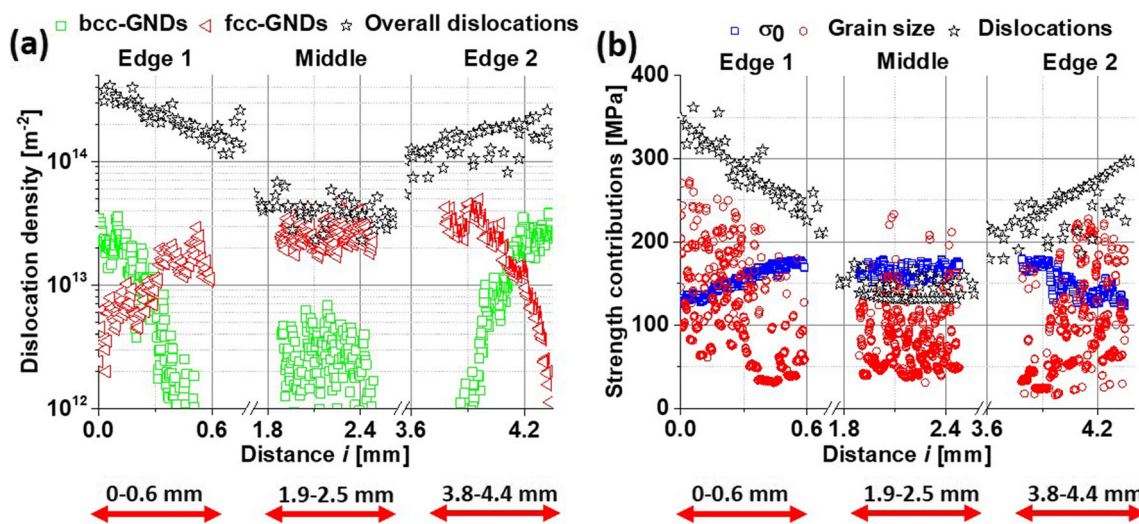
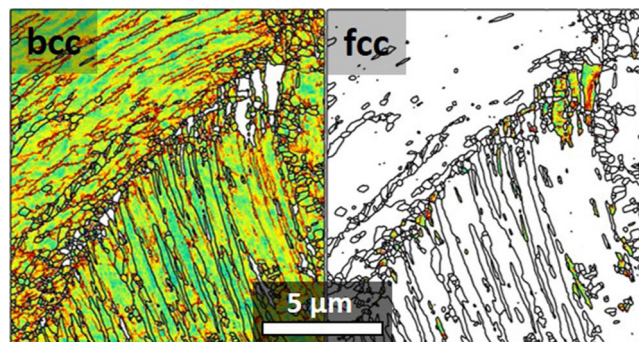


Fig. 7 Microstructure and hardening contributions. (a) Dislocation densities along the sheet thickness and (b) strength contributions across the material thickness

correspond to the martensite phase; however, when moving away 300 μm from this area, the austenite GNDs take on greater prominence and begin to grow until reaching values between  $1 \times 10^{13}$  and  $4 \times 10^{13} \text{ m}^{-2}$ , similar to the martensite at the edges. In addition to the discussion above, in the central zone, the GND values follow a more homogeneous distribution without significant variations on the sheet length,

although with higher magnitudes for austenite ( $3 \times 10^{13} \text{ m}^{-2}$ ) than for martensite ( $4.5 \times 10^{12} \text{ m}^{-2}$ ) that corroborates the lower degree of deformation in this area compared with the edge zones.

By knowing the magnitude of the dislocation densities, the different material strength contributions are obtained at each point of the sheet thickness. In this way, the equations that describe the strength evolution in each of the zones are as follow:



$$\sigma_{0i} = [\chi_i \cdot \sigma_{0-bcc} + (1-\chi_i) \cdot \sigma_{0-fcc}] \tag{6}$$

$$\sigma_{Di} = [\chi_i \cdot K_{bcc} \cdot D_i^{-1/2} + (1-\chi_i) \cdot K_{fcc} \cdot D_i^{-1/2}] \tag{7}$$

$$\sigma_{\rho i} = \alpha G M b \cdot \sqrt{\frac{1}{13.5} \cdot \left(\frac{H_{Vi} - H_{V0}}{\alpha G M b}\right)} \tag{8}$$

where the sub-index  $i$  refers to the strength value at any point of the sheet thickness. Thus, using Eqs. (6) to (8) and the values in Table 1, an evolution of each of the strength components is obtained. From Fig. 7b, it is verified that the most significant strength contributions come from the areas near the edges, forming a decreasing gradient as it moves away from the edge. Besides, dislocations appear as the most significant contribution in the three zones.

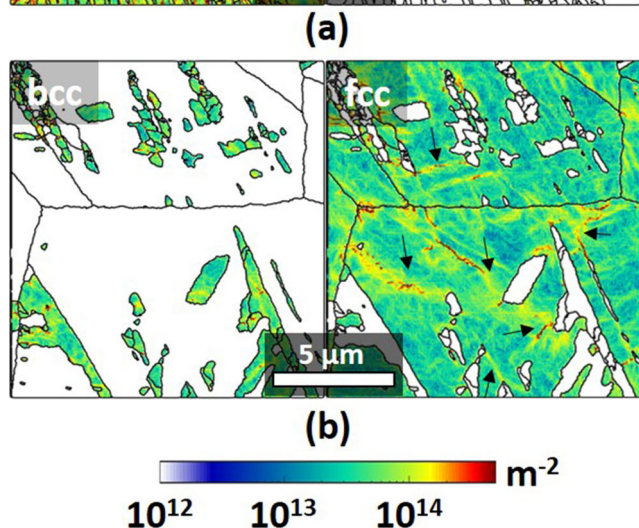
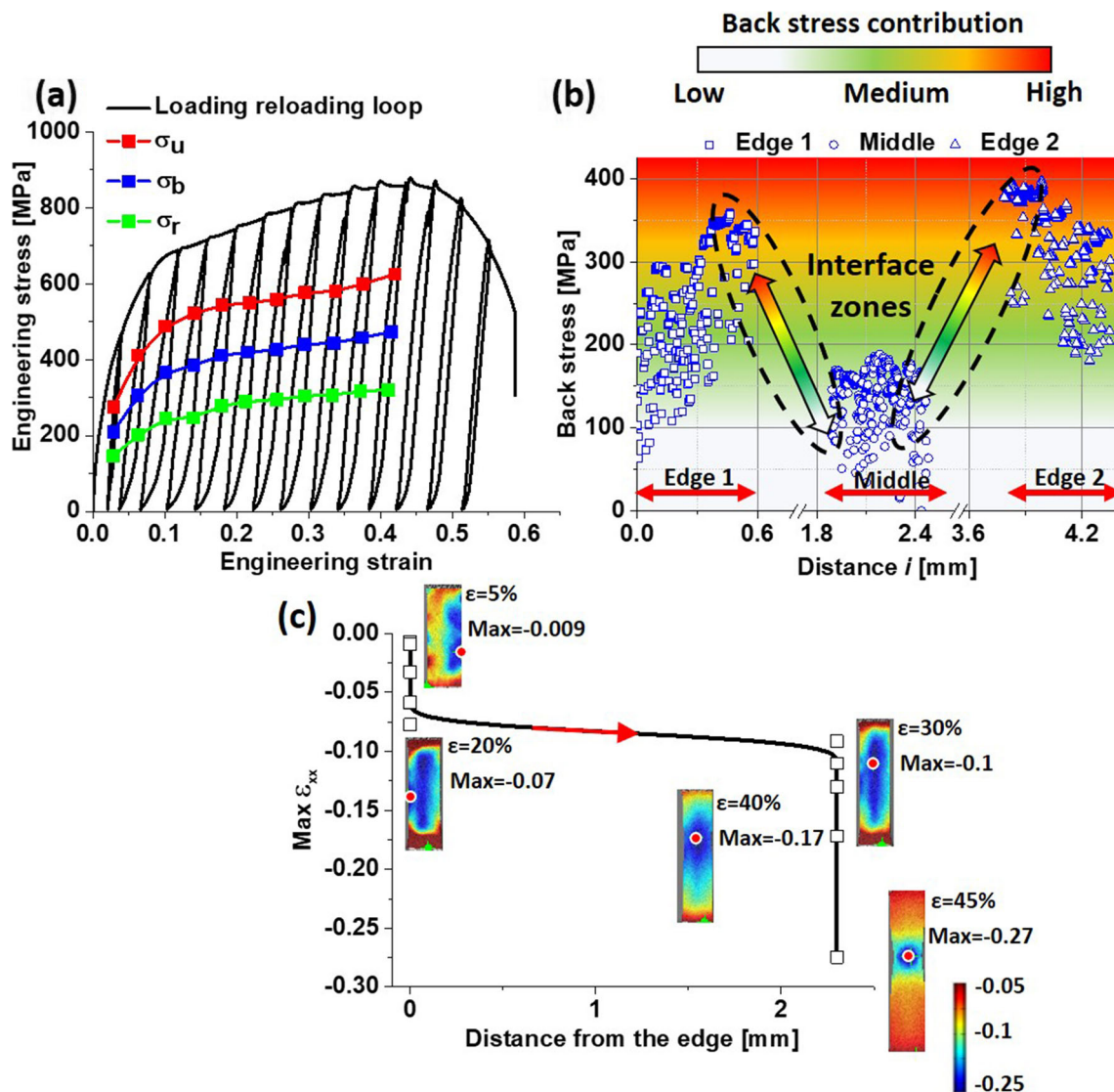


Figure 8 shows the GND maps are near the edge and in the middle zone. Figure 8a corroborates the larger presence of the martensite phase around the edge with higher dislocation densities than in the middle area of the sheet. On the other hand, Fig. 8b demonstrates that the middle zone is dominated by the more significant presence of austenite, demonstrating a GND arrangement different from that of the edge zone. GND pile-ups around the martensite islands can be seen in Fig. 8b, as indicated by the black arrows. This behavior also clarifies the existence of heterogeneity in the middle zone due to the

Fig. 8 GND maps around the (a) edge and (b) in the middle zone



**Fig. 9** Back stress and strain calculation. (a) Loading reloading loop and (b) back stress evolution along the sheet thickness, and (c) maximum strain  $\epsilon_{xx}$  component localization

interaction between the austenite and martensite phases. These two phases have different microstructural characteristics, e.g., marked differences in their grain sizes, which results in tougher (martensite) and more ductile areas (austenite). Several authors [2, 9] have explained that in the heterogeneous materials, the GNDs piled up in the soft zone generates a stress on the hard zone depending on the number of aligned dislocations giving rise to a new hardening mechanism. Therefore, Fig. 7a and Fig. 8b allow seeing that the material has a double heterogeneity. First, the heterogeneity induced by the ECASE process modifies the areas near the edges, and secondly, is the heterogeneity due to the manufacturing process that resulted in a distribution of martensite islands along with austenite grains as demonstrated by the initial material microstructure.

In addition to the different contributions mentioned above, the interactions which take place at the interfaces between hard and soft areas as a consequence of the strain partition give rise to a new hardening component known as back stress. Several researchers suggest that a good approximation of this contribution is obtained through a loading-unloading loop, as shown in Fig. 8a, and then using the following equation to calculate its magnitude [3, 4, 32]:

$$\sigma_b = (\sigma_u + \sigma_r)/2 \quad (9)$$

where  $\sigma_u$  and  $\sigma_r$  correspond to the unload and load yield stresses in each cycle, respectively. Figure 8a shows the back stress evolution, where it is appreciated that this contribution represents about 35% of the material yield stress. Taking into



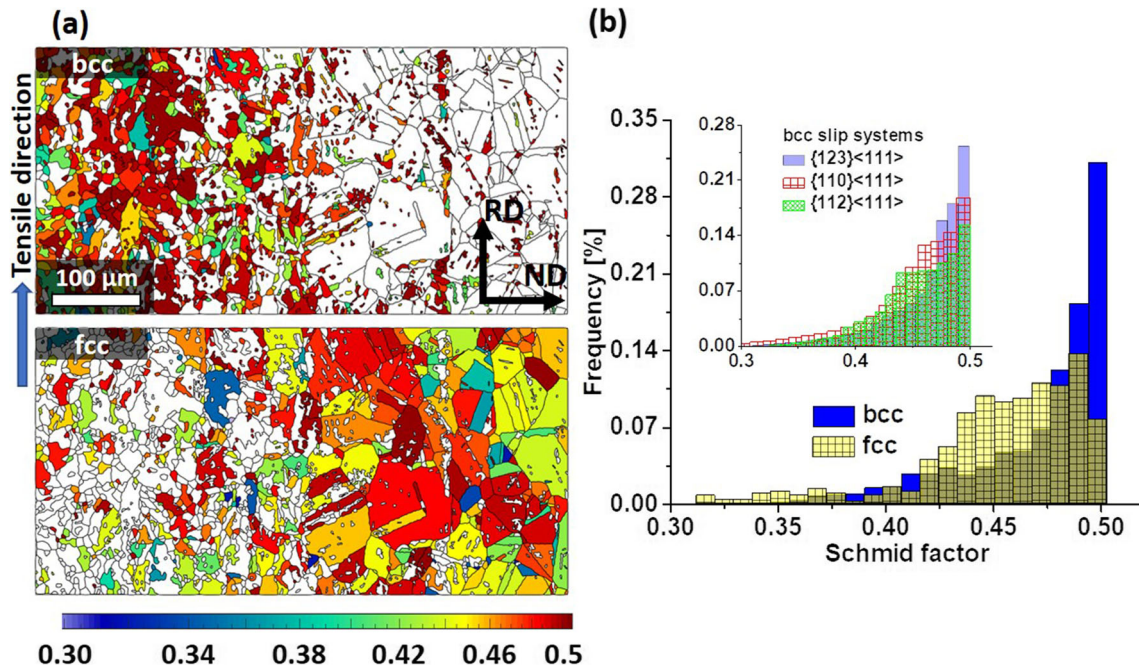


**Fig. 10** Schmid factor evolution around the sheet edge after 1 ECASE pass. (a) EBSD Schmid factor maps. (b) Schmid factor values for bcc and fcc phases after 1 ECASE pass

account this contribution to the overall material strength, the new equation describing the yield stress is [9]:

$$\sigma_{yi} = \sigma_{0i} + K \cdot D_i^{-1/2} + \alpha G M b \sqrt{\rho_{si} + \rho_{GNDi}} + \sigma_{bi} \quad (10)$$

Through Eq. (10), Fig. 8 b displays the back stress contribution and its evolution across the sheet thickness. This figure shows that the areas around the edges register the biggest contributions with higher values at the interfaces between the hard and soft areas than in the edges or middle regions, and it keeps good correlation with values obtained by the loading and unloading loop. The high back stress values in

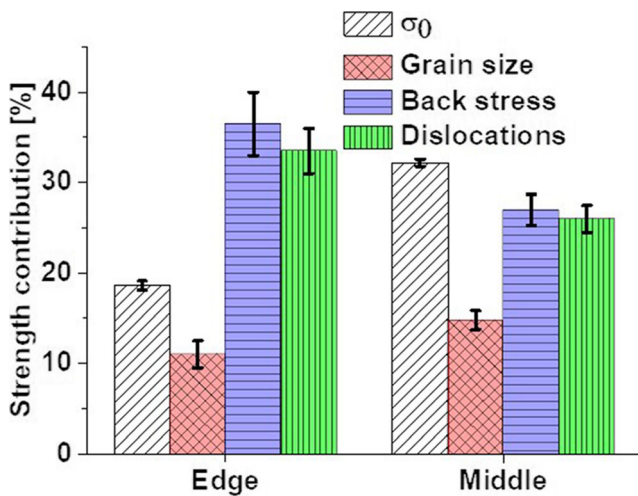


**Fig. 11** Strength contributions for each zone of the heterogeneous material

the edge vicinities correspond well with the high GND density in these areas, especially at the interfaces located around 600 microns from each edge. This observation is in good agreement with the research work of Park et al. [32] who also registered higher GND concentrations in the interfaces defining the material heterogeneity for a heterogeneous 304L austenitic steel with harmonic structure.

As a consequence of the material heterogeneity, Fig. 8 c demonstrates the strain partition, where initially, the maximum deformations in the  $\epsilon_{xx}$  component situate around the edge vicinities for tensile deformations lower than 20%. Beyond this point, higher deformations move towards the middle area until its final fracture at 45% of deformation. This situation demonstrates that the areas near the edge (hard-soft interface) withstand the highest deformations as a result of the interaction of geometrically necessary dislocations until they reach a balance between the two zones. Once the GND differences between the two zones are reduced, the deformation process continues like a homogeneous material.

To confirm the ease with which a material can flow, Fig. 9 shows the Schmid factor evolution in the area that encompasses the zone near the edge and the interface between the hard and soft regions. Therefore, the higher the Schmid factor, the easier the deformation will be. Through Fig. 9a, b, it is easy to identify that there are more grains of martensite with Schmid factors of 0.5 than the austenite phase, which is confirmed by Fig. 9b showing a peak with an approximate frequency of 35% for Schmid factors around 0.5, while austenite only reaches a fraction of ~14%. Also, in the inset of Fig. 9b,

it is shown that for the area near the edge (mostly bcc martensite), the most active system corresponds to  $\{123\} \langle 111 \rangle$  followed by the systems  $\{110\} \langle 111 \rangle$  and  $\{112\} \langle 111 \rangle$ , respectively. The high values of the Schmid factor in the tensile direction for the edge zone corroborate the observations of the deformation measurements, where material flows more easily in the edge vicinity than in the middle zone (Fig. 10).

Finally, Fig. 11 summarizes the different strength contributions of the heterogeneous material in each of the areas that comprise it. The main strength contribution around the edges is the back stress, with more than 35% and the dislocations with around 30% of the overall edge contribution. Conversely, the main contribution for the middle region is coming from the Peierls mechanism representing  $\sim 33\%$  of the strength followed closely by the back stress and dislocation contributions. This behavior demonstrates that although the most significant back stress contribution occurs in the border areas, there is also a significant contribution in the middle zone. The fact of the high back stress contribution in the middle zone is due to the presence of two phases (martensite and austenite) with different grain sizes and GND densities, generating a second heterogeneity in the material.

## 4 Conclusions

After having subjected a sheet-shaped heterogeneous austenitic stainless steel to plastic deformation at room temperature, the following conclusions summarize the main findings of this work:

The ECASE process produced a material with a gradient microstructure formed mainly by the heterogeneous distribution of phases, i.e., high amount of austenite in the nucleus, and a more considerable amount of martensite induced by deformation at the edge, different grain size distributions, and quite different dislocation densities between edges and the sheet core.

The high GND densities in the edge vicinities generated a plastic gradient that allowed to obtain a material with a good strength-ductility ratio, where the regions near the edge initially assumed larger strains than the sheet core as evidenced by the Schmid factor and the strain maps.

The different strength contributions across the plate thickness demonstrated higher values around the edge region than in the middle zone. All of them, except the back stress, decrease as they moved away from the edges. While, in the central area, all the contributions behave homogeneously.

The most significant strength contributions of the material correspond with the regions near the edge, being the back stress and dislocation contributions the most important. The back stress mechanism also plays an essential role in the middle zone, being the second strength contribution after the

Peierls mechanism due to the second heterogeneity generated between austenite and martensite before ECASE.

**Acknowledgments** Authors also thank professors Raúl Bolmaro and Martina Avalos for their help with EBSD characterization.

**Credit authorship statement** Jairo Alberto Muñoz: Investigation, methodology, formal analysis, writing original draft, writing review and editing, data curation Alexander Komissarov: Supervision, funding acquisition, resources, investigation, project administration.

**Funding information** JAMB thanks the Latin-American Postdoctoral scholarship (Grant number CONICET D 4263) received from the Argentine Ministry of Science, Technology and Productive Innovation and the National Council of Scientific and Technical Research (CONICET).

The authors gratefully acknowledge the financial support of the Ministry of Science and Higher Education of the Russian Federation in the framework of Increase Competitiveness Program of NUST «MISIS» (№ K4-2019-045), implemented by a governmental decree dated 16th of March 2013, N 211.

## Compliance with ethical standards

**Conflict of interest** The authors declare that they have no conflict of interest.

## References

1. Ma E, Zhu T (2017) Towards strength–ductility synergy through the design of heterogeneous nanostructures in metals. *Mater Today* 20:323–331. <https://doi.org/10.1016/j.mattod.2017.02.003>
2. Wu X, Zhu Y (2017) Heterogeneous materials: a new class of materials with unprecedented mechanical properties. *Mater Res Lett* 5:527–532. <https://doi.org/10.1080/21663831.2017.1343208>
3. Wu X, Yang M, Yuan F, Wu G, Wei Y, Huang X, Zhu Y (2015) Heterogeneous lamella structure unites ultrafine-grain strength with coarse-grain ductility. *Proc Natl Acad Sci U S A* 112:14501–14505. <https://doi.org/10.1073/pnas.1517193112>
4. Shukla S, Choudhuri D, Wang T, Liu K, Wheeler R, Williams S, Gwalani B, Mishra RS (2018) Hierarchical features infused heterogeneous grain structure for extraordinary strength-ductility synergy. *Mater Res Lett* 6:676–682. <https://doi.org/10.1080/21663831.2018.1538023>
5. S. Attarilar, M.T. Salehi, K.J. Al-Fadhlah, F. Djavanroodi, M. Mozafari, Functionally graded titanium implants: characteristic enhancement induced by combined severe plastic deformation, *PLoS One*. 14 (2019). doi:10.1371/journal.pone.0221491.
6. Zheng R, Bhattacharjee T, Gao S, Gong W, Shibata A, Sasaki T, Hono K, Tsuji N (2019) Change of deformation mechanisms leading to high strength and large ductility in Mg-Zn-Zr-Ca alloy with fully recrystallized ultrafine grained microstructures. *Sci Rep* 9. <https://doi.org/10.1038/s41598-019-48271-5>
7. Wang Y, Yang M, Ma X, Wang M, Yin K, Huang A, Huang C (2018) Improved back stress and synergetic strain hardening in coarse-grain/nanostructure laminates. *Mater Sci Eng A* 727:113–118. <https://doi.org/10.1016/j.msea.2018.04.107>
8. Yang M, Pan Y, Yuan F, Zhu Y, Wu X (2016) Back stress strengthening and strain hardening in gradient structure. *Mater Res Lett* 4: 145–151. <https://doi.org/10.1080/21663831.2016.1153004>
9. Li J, Lu W, Chen S, Liu C (2019) Revealing extra strengthening and strain hardening in heterogeneous two-phase nanostructures.

- Int J Plast 102626:102626. <https://doi.org/10.1016/j.ijplas.2019.11.005>
10. Duan J, Wen H, Zhou C, He X, Islamgaliev R, Valiev R (2019) Discontinuous grain growth in an equal-channel angular pressing processed Fe-9Cr steel with a heterogeneous microstructure. *Mater Charact* 110004:110004. <https://doi.org/10.1016/J.MATCHAR.2019.110004>
  11. Jamaljan M, Hamid M, De Vincentis N, Buck Q, Field DP, Zbib HM (2019) Creation of heterogeneous microstructures in copper using high-pressure torsion to enhance mechanical properties. *Mater Sci Eng A* 756:142–148. <https://doi.org/10.1016/j.msea.2019.04.024>
  12. Wang X, Li YS, Zhang Q, Zhao YH, Zhu YT (2017) Gradient structured copper by rotationally accelerated shot peening. *J Mater Sci Technol* 33:758–761. <https://doi.org/10.1016/j.jmst.2016.11.006>
  13. Spadaro L, Hereñú S, Strubbia R, Gómez Rosas G, Bolmaro R, Rubio González C (2020) Effects of laser shock processing and shot peening on 253 MA austenitic stainless steel and their consequences on fatigue properties. *Opt Laser Technol* 122:105892. <https://doi.org/10.1016/j.optlastec.2019.105892>
  14. Amanov A, Karimbaev R, Maleki E, Unal O, Pyun YS, Amanov T (2019) Effect of combined shot peening and ultrasonic nanocrystal surface modification processes on the fatigue performance of AISI 304. *Surf Coat Technol* 358:695–705. <https://doi.org/10.1016/j.surfcoat.2018.11.100>
  15. Chen M, Jiang C, Xu Z, Zhan K, Ji V (2019) Experimental study on macro- and microstress state, microstructural evolution of austenitic and ferritic steel processed by shot peening. *Surf Coat Technol* 359: 511–519. <https://doi.org/10.1016/j.surfcoat.2018.12.097>
  16. Jamaljan M, Field DP (2019) Effects of shot peening parameters on gradient microstructure and mechanical properties of TRC AZ31. *Mater Charact* 148:9–16. <https://doi.org/10.1016/j.matchar.2018.12.001>
  17. Jamaljan M, Field DP (2019) Gradient microstructure and enhanced mechanical performance of magnesium alloy by severe impact loading. *J Mater Sci Technol* 36:45–49. <https://doi.org/10.1016/j.jmst.2019.06.013>
  18. Muñoz JA, Higuera OF, Tartalini V, Risso P, Avalos M, Bolmaro RE (2019) Equal channel angular sheet extrusion (ECASE) as a precursor of heterogeneity in an AA6063-T6 alloy. *Int J Adv Manuf Technol* 102:3459–3471. <https://doi.org/10.1007/s00170-019-03425-7>
  19. Cheng YQ, Chen ZH, Xia WJ, Zhou T (2007) Effect of channel clearance on crystal orientation development in AZ31 magnesium alloy sheet produced by equal channel angular rolling. *J Mater Process Technol* 184:97–101. <https://doi.org/10.1016/j.jmatprotec.2006.11.010>
  20. Hassani FZ, Ketabchi M (2011) Nano grained AZ31 alloy achieved by equal channel angular rolling process. *Mater Sci Eng A* 528: 6426–6431. <https://doi.org/10.1016/j.msea.2011.05.024>
  21. Saray O, Purcek G, Karaman I (2010) Principles of equal-channel angular sheet extrusion (ECASE): application to IF-steel sheets. *Rev Adv Mater Sci* 25:42–51
  22. Michler T (2016) Austenitic stainless steels, in: Ref. Modul. *Mater. Sci. Mater. Eng.* Elsevier. <https://doi.org/10.1016/B978-0-12-803581-8.02509-1>
  23. McGuire MF (2001) Austenitic Stainless Steels. In: Buschow KJH, Cahn RW, Flemings MC, Iilschner B, Kramer EJ, Mahajan S, Veyssière P (eds) *Encycl. Mater. Sci. Technol.* Elsevier, Oxford, pp 406–410. <https://doi.org/10.1016/B0-08-043152-6/00081-4>
  24. de Abreu HFG, de Carvalho SS, de Lima Neto P, dos Santos RP, Freire VN, de O. Silva PM, Tavares SSM (2007) Deformation induced martensite in an AISI 301LN stainless steel: characterization and influence on pitting corrosion resistance. *Mater Res* 10: 359–366 [http://www.scielo.br/scielo.php?script=sci\\_arttext&pid=S1516-14392007000400007&nrm=iso](http://www.scielo.br/scielo.php?script=sci_arttext&pid=S1516-14392007000400007&nrm=iso)
  25. Akopyan TK, Belov NA, Aleshchenko AS, Galkin SP, Gamin YV, Gorshenkov MV, Cheverikin VV, Shurkin PK (2019) Formation of the gradient microstructure of a new Al alloy based on the Al-Zn-Mg-Fe-Ni system processed by radial-shear rolling. *Mater Sci Eng A* 746:134–144. <https://doi.org/10.1016/j.msea.2019.01.029>
  26. Li Wang Y, Molotnikov A, Diez M, Lapovok R, Kim HE, Tao Wang J, Estrin Y (2015) Gradient structure produced by three roll planetary milling: numerical simulation and microstructural observations. *Mater Sci Eng A* 639:165–172. <https://doi.org/10.1016/j.msea.2015.04.078>
  27. Schramm RE, Reed RP (1975) Stacking fault energies of seven commercial austenitic stainless steels. *Metall Trans A* 6:1345–1351
  28. Lu J, Hultman L, Holmström E, Antonsson KH, Grehk M, Li W, Vitos L, Golpayegani A (2016) Stacking fault energies in austenitic stainless steels. *Acta Mater* 111:39–46. <https://doi.org/10.1016/j.actamat.2016.03.042>
  29. Lee Y-K, Lee S-J, Han J (2016) Critical assessment 19: stacking fault energies of austenitic steels. *Mater Sci Technol* 32:1–8. <https://doi.org/10.1080/02670836.2015.1114252>
  30. Iwahashi Y, Wang J, Horita Z, Nemoto M, Langdon TG (1996) Principle of equal-channel angular pressing for the processing of ultra-fine grained materials. *Scr Mater* 35:143–146. [https://doi.org/10.1016/1359-6462\(96\)00107-8](https://doi.org/10.1016/1359-6462(96)00107-8)
  31. Zheng ZJ, Liu JW, Gao Y (2017) Achieving high strength and high ductility in 304 stainless steel through bi-modal microstructure prepared by post-ECAP annealing. *Mater Sci Eng A* 680:426–432. <https://doi.org/10.1016/j.msea.2016.11.004>
  32. Park HK, Ameyama K, Yoo J, Hwang H, Kim HS (2018) Additional hardening in harmonic structured materials by strain partitioning and back stress. *Mater Res Lett* 6:261–267. <https://doi.org/10.1080/21663831.2018.1439115>
  33. Taylor GI The mechanism of plastic deformation of crystals. Part I.—Theoretical. *Proc R Soc Lond Ser A Contain Pap A Math Phys Charact* 145(1934):362–387
  34. Odnobokova M, Belyakov A, Kaibyshev R (2015) Development of nanocrystalline 304L stainless steel by large strain cold working. *Metals (Basel)* 5:656–668. <https://doi.org/10.3390/met5020656>
  35. Belyakov A, Tsuzuki K, Kimura Y, Mishima Y (2009) Tensile behaviour of submicrocrystalline ferritic steel processed by large-strain deformation. *Philos Mag Lett* 89:201–212. <https://doi.org/10.1080/09500830902748298>
  36. Muñoz JA, Higuera OF, Cabrera JM (2017) Microstructural and mechanical study in the plastic zone of ARMCO iron processed by ECAP. *Mater Sci Eng A* 697:24–36. <https://doi.org/10.1016/j.msea.2017.04.108>
  37. Karavaeva M, Abramova M, Enikeev N, Raab G, Valiev R Superior strength of austenitic steel produced by combined processing, including equal-channel angular pressing and rolling. *Metals (Basel)* 6(2016):310. <https://doi.org/10.3390/met6120310>
  38. Hardin TJ, Adams BL, Fullwood DT, Wagoner RH, Homer ER (2013) Estimation of the full Nye’s tensor and its gradients by micro-mechanical stereo-inference using EBSD dislocation microscopy. *Int J Plast* 50:146–157. <https://doi.org/10.1016/j.ijplas.2013.04.006>